Contactless magnetoresistance studies of Co/Cu multilayers using the infrared magnetorefractive effect

M. Vopsaroiu, D. Bozec,* J. A. D. Matthew, and S. M. Thompson
Department of Physics, University of York, Heslington YO10 5DD, United Kingdom

C. H. Marrows and M. Perez†
School of Physics and Astronomy, University of Leeds, Leeds LS2 9JT, United Kingdom
(Received 11 February 2004; revised manuscript received 1 June 2004; published 21 December 2004)

The magnetotransport properties of giant magnetoresistive Co/Cu multilayers are studied with the magnetorefractive effect: a noncontact technique, which uses infrared electromagnetic radiation. Four Co/Cu samples were analyzed with the structure $(Co_{15.5\ Å}/Cu_x)_{25}$ which exhibit magnetoresistance values from 1.9 to 65 %. The magnetorefractive curves were modeled using the complex dielectric function as derived by Jacquet and Valet [J. C. Jacquet and T. Valet, *Magnetic Ultrathin Films, Multilayer and Surfaces*, edited by E. Marinero (Materials Research Society, Pittsburgh, 1995)]. The shape and magnitude of the curves were found to be very sensitive to the interface scattering lifetime. This classical model is successful in simulating the long wavelength behavior, but is not able to reproduce the correct shape or sign at short wavelengths where the band structure of the materials becomes important. The good agreement at long wavelengths between electrical magnetotransport measurements and the noncontact magnetorefractive effect demonstrates the possibilities of using infrared reflection spectroscopy for the characterization of giant magnetoresistive systems.

DOI: 10.1103/PhysRevB.70.214423 PACS number(s): 75.47.−m, 75.70.Cn, 78.20.Ls, 73.50.Bk

I. INTRODUCTION

Important advances in magnetism such as the discovery of oscillatory exchange coupling in metallic multilayers and the exchange bias effect in FM/AFM bilayers have triggered the rapid development of a class of materials and devices presenting magnetotransport phenomena. The key property of these materials is the reduction of their electrical resistivity when a magnetic field is applied. The most common method of measuring magnetoresistance involves passing an electrical current through the sample via a four point probe. However, this is not always convenient since electrical measurements often result in surface damage or sample contamination and they are not generally suitable for *in situ* experiments. Jaquet and Valet[1] (hereafter referred to as JV) proposed and demonstrated an alternative noncontact method for the measurement of magnetotransport effects using electromagnetic radiation. The method is based on the magnetorefractive effect (MRE).[1] The MRE is the variation of the refractive index (via the dielectric function) of a material due to a change in its conductivity at infrared (IR) frequencies when a magnetic field is applied. The MRE is useful in magnetoresistive materials because at those wavelengths the optical transport properties in metals depend mainly on the electron transitions within the conduction band (i.e., the intraband transitions). This is in contrast to the magneto-optic, Faraday, and nonlinear effects in the visible light regime where the interband transitions dominate the response.[2,3] A direct measure of the changes in the dielectric properties of a material can be performed by determining its reflection/transmission coefficients. Hence, infrared transmission/reflection spectroscopy as a function of the applied magnetic field can provide a direct tool for probing the spin-dependent conductivity in giant magnetoresistive (GMR), tunnel magnetoresistive (TMR), and colossal magnetoresistive (CMR) materials. Since its discovery in 1995,[1] the MRE has been successfully used to study a wide variety of MR materials such as trilayers[4] granular systems Co_xAg_{1-x},[5,6] $(CoFe)_x(Al_2O_3)_{1-x}$,[7,8] manganite nanocomposites,[9] commercial spin valves[10,11] and LaSrMnO perovskites.[12]

In this paper we measure the MRE of Co/Cu, a previously uninvestigated multilayer system characterized by variation of antiferromagnetic coupling with Cu layer thickness, and demonstrate its correlation with conventional magnetotransport measurements. In addition to adding to the limited range of investigations of MRE on multilayers, the paper widens the insights of JV in a number of ways. Measurements are made in reflection, the most likely mode for practical remote sensing of GMR, in contrast to the transmission experiments on multilayers presented by JV, and the wavelength range is extended to confirm the change of sign of the reflection MRE in the near infrared. A simple theoretical model of the spin dependent complex dielectric function based on the original JV approach is used to simulate the MRE demonstrating the strong sensitivity of the wavelength dependence profile to material parameters. Finally, the results are compared to a fundamental theory of the relation between MRE and GMR emphasizing the effects of spin-dependent superlattice band structure on the phenomena.[13]

II. EXPERIMENTAL PROCEDURE

A set of four Co/Cu multilayers with different Cu thickness were prepared by dc magnetron sputtering at The University of Leeds. The base pressure was 20 nTorr and the samples were deposited on Si substrates 340 microns thick. A Cr seed layer was deposited at room temperature in a weak bias field of approximately 200 Oe, which introduces a very

TABLE I. Summary of the Co/Cu multilayer samples with their structural, magnetic, and current-in-plane (CIP) magnetotransport parameters.

Sample code	A	B	C	D
t_{Cu} (Å)	7.5	10	16	16.7
Total thickness (Å)	679	742	893	911
Cr(105 Å)/{Co(15.5 Å)/t_{Cu}}×25				
$m_0=(M/M_s)_{H=0}$	0.1	0.95	0.96	0.78
Experimental (CIP) GMR (%)	65	2.8	1.9	10.8
Experimental (−MRE) (%) measured at 20 μm	5.4	0.2	0.25	0.6

small in-plane anisotropy. The structure of the Co/Cu multilayers was $Cr_{105\ Å}/[(Co_{15.5\ Å}/Cu_x)]_{25}$, where x was varied from 7.5 to 16.7 Å in order to vary the interlayer exchange coupling from ferromagnetic to antiferromagnetic and hence vary the GMR. Sample details and experimental results are presented in Table I.

All measurements were carried out at room temperature. Magnetic measurements were made using a vibrating sample magnetometer and electrical magnetotransport measurements were made with the dc current inplane (CIP) using a four-point in-line probe with a 1 mA applied current parallel to the applied magnetic field, maximum value of ±9 kOe. Numerical evaluation of the GMR effect was obtained using the relation

$$\mathrm{GMR}(\%) = \frac{\rho(H) - \rho(H_{\max})}{\rho(H_{\max})} \times 100, \qquad (1)$$

where $\rho(H)$ is the resistance of the sample in an applied magnetic field (H) and $\rho(H_{\max})$ is the resistance in the maximum applied magnetic field, in this case ±9 kOe.

III. EXPERIMENTAL RESULTS

The experimental GMR for all the samples was symmetric in an applied field. The maximum values varied from 1.9 to 65 % depending on the Cu layer thickness and are presented in Table I and Fig. 1. Sample A exhibits behavior typical of strong antiferromagnetic coupling with a slow approach to saturation in an applied field of ±9 kOe and no hysteresis. Samples B and C are ferromagnetically coupled with rapid magnetic switching, a high remanent magnetisation and very low GMR. Sample D is intermediate between these extremes.

MRE measurements were performed using a Nicolet Fourier Transform IR reflection spectrometer with 0.25 μm resolution and a liquid nitrogen-cooled HgCdTe detector. Room-temperature IR spectra were collected between 2.5 and 20 μm in zero magnetic field and in a magnetic field of ±13 kOe perpendicular to the plane of incidence. Both experimental and theoretical MRE studies show that p-polarized infrared radiation gives a larger MRE effect, therefore the MRE spectra were obtained in p-polarized light using a KRS-5 grid polarizer, for an incidence angle set at $\theta=75°\pm2^0$ with respect to the surface normal. The MRE infrared reflection spectra for a specific applied field show the percentage change in the reflection of IR light due to the application of the magnetic field. Experimental MRE spectra obtained in a saturating 13 kOe applied magnetic field and calculated according to Eq. (2) are shown as a function of wavelength in Fig. 2:

$$\mathrm{MRE}(\%) = \frac{0.5(S_3 + S_1) - S_2}{S_2} \times 100, \qquad (2)$$

where S_1, S_2, and S_3 are three consecutive spectra; S_1 and S_3 are taken in zero applied field and S_2 is the spectrum acquired in an applied magnetic field. S_1 and S_3 are averaged in order to take into account any variations in the background, which change linearly with time such as thermal drift.

IV. EXPERIMENTAL DISCUSSION

The MRE spectra for the Co/Cu multilayers show a similar shape to those observed in CoAg granular GMR films.[5,6] They have a broad positive peak in the MRE at short wavelengths followed by a crossover into a reduced reflection region resulting in negative MRE at longer wavelengths. This increase in the reflectivity in an applied field is consistent with the increase in electrical conductivity resulting

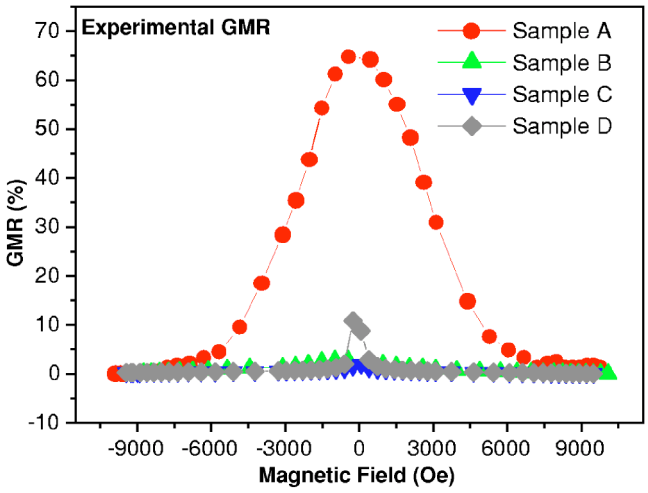

FIG. 1. (Color online) Experimental CIP GMR data of Co/Cu samples.

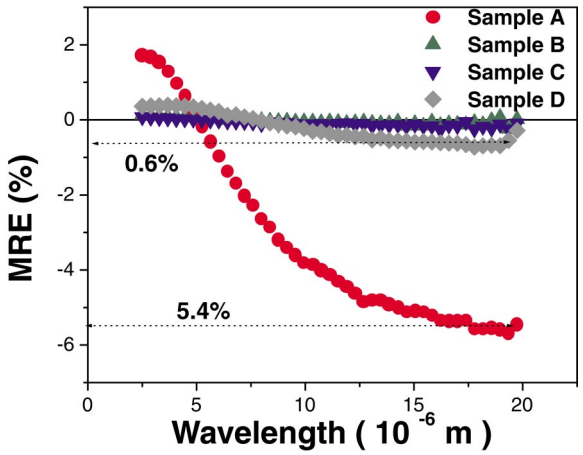

FIG. 2. (Color online) Experimental MRE spectra in *p*-polarized IR light of all four Co/Cu samples measured in a saturating magnetic field of +13 kOe.

from the magnetically induced modification of the scattering of the Drude-like free electrons. It is immediately clear that sample A with the largest GMR also exhibits the largest MRE. In addition, the wavelength at which the crossover from positive to negative MRE occurs increases with increasing t_{Cu}. In order to make a comparison between the MRE and GMR, the MRE at a wavelength of 20 μm is used. This is usually around the lowest point of the spectrum and far away from the short wavelength region where interband transitions are important. However, the precise choice of the wave-length changes only the absolute value of the MRE leaving the excellent correlation with the GMR intact. In Fig. 3, MRE values are presented along with the GMR values of Table I as a function of the Cu layer thickness t_{Cu}.

Figure 3 demonstrates the highly correlation degree between the electrically measured GMR and the optically measured MRE. The GMR is an entirely electrical measurement in which direct electrical conductivity measurements are made while the MRE is an IR technique for determining the

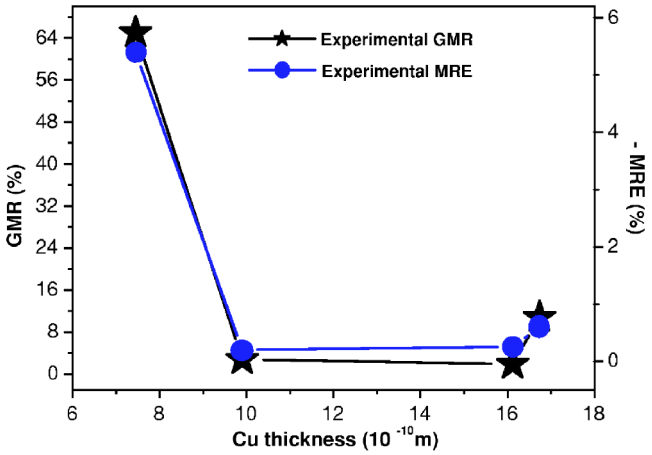

FIG. 3. (Color online) Correlation between experimental GMR data at 9 kOe and experimental MRE values measured at 20 μm in a 13 kOe applied magnetic field, represented as a function of the Cu thickness.

change in the optical conductivity due to the application of a magnetic field, which in turn affects the reflectivity of the sample. The correlation factor between the two measurements varies as a function of the sample spin-independent resistivity, the incidence angle and the precise wavelength at which MRE is measured.[6] In the comparison presented in Table I and Fig. 3, the wavelength is precisely defined while the angle of incidence may vary slightly from sample to sample. Also the spin-independent resistivity does vary significantly between the samples and this influences the correlation factor even in the Hagen-Rubens limit.[6]

V. SIMULATIONS

A theoretical effective medium model has been developed in order to simulate the MRE spectra of GMR materials. The overall thickness of the Co/Cu layers is significantly greater than the attenuation length of the radiation, so that the Cr underlayer is not sampled. On the other hand, the individual Co/Cu layer thicknesses are much less than the attenuation length. It is therefore plausible to treat the Co/Cu layers structure as an effective medium with scattering parameters and effective dielectric function obtained by averaging the material characteristics appropriately. The objective of the simulation with this simple model is not to make a perfect fit to the MRE data but to give guidance in using the observed correlation between GMR and MRE data. The model uses the modified complex Drude dielectric function as introduced by Jacquet and Valet[1]

$$\varepsilon(\omega,m) = \varepsilon_r + i\varepsilon_a = \varepsilon_{\mathrm{st}} + \left(\frac{\omega_p}{\omega}\right)^2 \frac{i\omega\tau_{\mathrm{sal}}}{1 - i\omega\tau_{\mathrm{sal}}} \times \left(1 + \frac{m^2\beta_{\mathrm{sal}}{}^2}{(1 - i\omega\tau_{\mathrm{sal}})^2 - m^2\beta_{\mathrm{sal}}{}^2}\right), \quad (3)$$

where ε is the complex dielectric function of the material, $\varepsilon_{\mathrm{st}}$ is the frequency-independent contribution to the dielectric function which is 1 in the Drude model and 3.5 in the modified Drude model, ω_p is the quasi-free-electron plasma frequency, ω is the angular frequency of the incident light, ε_a and ε_r are the imaginary and real parts of the complex dielectric function, respectively, and $m = M/M_s$ is the normalized magnetization that takes into account the reduced magnetic alignment of the magnetic layers below magnetic saturation. The self-averaged relaxation time τ_{sal} and spin asymmetry β_{sal} will be discussed in more detail below. This formula differs slightly from that of JV in using the more common relation between the frequency-dependent conductivity $\sigma(\omega)$ and the dc conductivity σ_0 (Refs. 14 and 15) $\sigma(\omega) = \sigma_0/(1 - i\omega\tau)$ rather than a plus sign in the denominator. There are no differences in the predictions of the simulation and they are consistent with the alternative formalism of Granovskii.[7] The dielectric function describing samples in zero applied magnetic field has the same form as Eq. (3) except that m is replaced by $m_0 = (M/M_s)_{H=0}$, which is the remanent normalized magnetization and can have values from 0 to 1. The m_0 values were extracted from the experimental hysteresis curves after separating out the contribution to the hysteresis from domain rotation (see Table I). $\tau_{\mathrm{sal}}{}^{-1}$ is

TABLE II. Summary of the simulation parameters.

Sample code	A	B	C	D
Volume fraction of Co/Cu interface C_i	0.49	0.44	0.35	0.34
Volume fraction of Co ferromagnet C_f	0.46	0.41	0.33	0.32
Volume fraction of non magnetic Cu, Cn	0.05	0.15	0.32	0.34
Average spin asymmetry constant β_{sal}	0.77	0.76	0.74	0.73
Average scattering time $\tau_{\mathrm{sal}} \times 10^{-15}$ s^{-1}	3.2	3.5	4.2	4.3
−MRE (%) at 20 μm from simulation of MRE (λ)	5.4	0.56	0.36	1.6

the average scattering rate in the self-averaging limit,[16,17] defined as the scattering rate averaged over a period equal to the bilayer period in the multilayer:

$$\tau_{\mathrm{sal}}^{-1} = \frac{1}{L}\int \frac{1}{\tau(z)}dz, \tag{4}$$

where L is the length of the sample in the z direction. β_{sal} is the average spin asymmetry constant also obtained in the self-average limit (SAL) formalism as derived in Ref. 1 and defined as

$$\tau_{\mathrm{sal}}^{\uparrow\downarrow} = \frac{\tau_{\mathrm{sal}}}{1 \pm \beta_{\mathrm{sal}} m}, \tag{5}$$

where $\tau_{\mathrm{sal}}^{\uparrow\downarrow}$ represents the average spin-dependent scattering rate for up-spin and down-spin, respectively, and $\tau_{\mathrm{sal}}^{-1} = (\tau_{\mathrm{sal}}^{\uparrow -1} + \tau_{\mathrm{sal}}^{\downarrow -1})/2$. In order to evaluate τ_{sal} and β_{sal}, the spin-independent scattering time in the ferromagnet is defined as τ_f, the spin-independent scattering time in the nonmagnetic layers as τ_n, and the spin-independent scattering time at the interface as τ_i. Assuming that the two types of carriers (spin-up and spin-down) can suffer spin dependent scattering at both the interface and in bulk, then the spin-dependent scattering times at the interface and in the bulk are defined in a similar way to Eq. (5) and as in Ref. 18:

$$\tau_f^{\uparrow\downarrow} = \frac{\tau_f}{1 \pm \beta m}, \tag{6}$$

$$\tau_i^{\uparrow\downarrow} = \frac{\tau_i}{1 \pm \gamma m}, \tag{7}$$

where β is the spin asymmetry coefficient of the bulk ferromagnetic layers and γ is the spin asymmetry coefficient of the interfacial layer. Defined at saturation magnetization ($m=1$), both parameters β and γ represent a measure of the degree of spin-dependent scattering due to the magnetic polarization. It is also assumed that there is no spin-dependent scattering in the nonmagnetic Cu layers. β and γ were introduced by Valet and Fert in order to model the spin-dependent scattering in GMR multilayers in the framework of the independent spin-up $\uparrow$ and spin-down $\downarrow$ current channels.[18] β and γ can have fractional values between 0 to 1 and they are usually obtained by fitting the theoretical relations with experimental GMR/MRE data. A value of $\beta=0$ means that there is spin dependence from interface scattering only, while a value of $\gamma=0$ means that the system exhibits spin dependence from bulk scattering only. By performing the integration in Eq. (4) for both spin-up and spin-down, and using Eqs. (5)–(7), the following equations are obtained for τ_{sal} and β_{sal}:

$$\frac{1}{\tau_{\mathrm{sal}}} = \frac{c_i}{\tau_i} + \frac{c_f}{\tau_f} + \frac{1 - c_i - c_f}{\tau_n}, \tag{8}$$

$$\beta_{\mathrm{sal}} = \tau_{\mathrm{sal}} \times \left(\gamma \frac{c_i}{\tau_i} + \beta \frac{c_f}{\tau_f} \right), \tag{9}$$

where c_f, c_n, and c_i are the volume fractions of ferromagnetic material, nonmagnetic material, and the interfacial region, respectively ($c_f + c_n + c_i = 1$). Parameter values that give reasonable fits to the MRE are given in Table II. Their physical significance will be discussed later in this section.

Assuming a single reflection of the infrared radiation at the air/effective medium interface, the infrared reflectivity R of the metallic GMR sample can be modeled by using the Fresnel equations derived for s and p polarized light:

$$R_{s,p} = |r_{s,p}|^2, \tag{10}$$

where $r_{s,p}$ are the Fresnel reflection coefficients for s and p polarized light, respectively. As mentioned in Sec. II we have performed both the experiments and the simulations for p-polarized IR light, for which we have derived the theoretical relation for the reflectivity of a GMR sample in an applied magnetic field as

$$R_p(H) = R(H) = \left| \frac{\cos\theta\varepsilon(\omega,m) - \sqrt{\varepsilon(\omega,m) - \sin^2\theta}}{\cos\theta\varepsilon(\omega,m) + \sqrt{\varepsilon(\omega,m) - \sin^2\theta}} \right|^2 \tag{11}$$

which in this case is also a saturating magnetic field ($m=1$). The theoretical relation for the reflectivity of a GMR sample in zero applied magnetic field is

$$R_p(0) = R(0) = \left| \frac{\cos\theta\varepsilon(\omega,m_0) - \sqrt{\varepsilon(\omega,m_0) - \sin^2\theta}}{\cos\theta\varepsilon(\omega,m_0) + \sqrt{\varepsilon(\omega,m_0) - \sin^2\theta}} \right|^2, \tag{12}$$

where $\varepsilon(\omega,m)$ and $\varepsilon(\omega,m_0)$ are given by relation (3) and θ is the incident angle. This is a more convenient form of the Fresnel coefficients for metallic systems than the more usual representation in terms of n and k.[19] The theoretical MRE was then computed in the same way as for the experimental definition of the MRE [Eq. (2)] and using the relations (11)

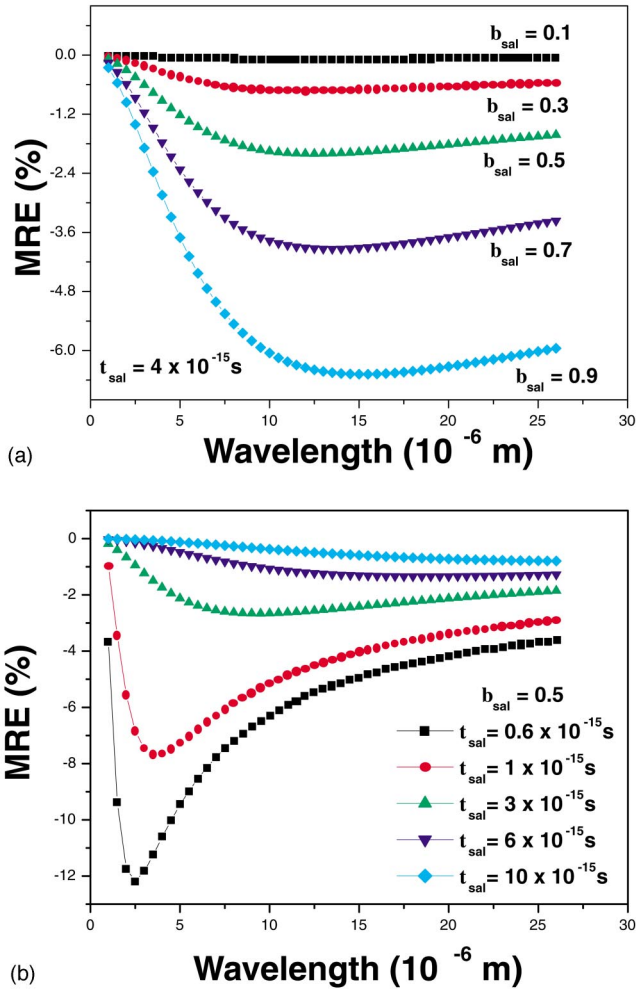

FIG. 4. (Color online) Simulation of (a) MRE vs wavelength at constant $\tau_{sal}=4\times10^{-15}$ s for different values of β_{sal} and (b) MRE vs wavelength at constant $\beta_{sal}=0.5$ and different values of τ_{sal}.

and (12) combined with the Drude modified dielectric function (3):

$$\mathrm{MRE}(\%)=\frac{R(0)-R(H)}{R(H)}\times 100, \tag{13}$$

where $R(0)$ is given by Eq. (12) and $R(H)$ is given by Eq. (11). The infrared wavelength was varied between 2 to 20 μm and the angle of incidence kept constant at $\theta=75°$ as in the experiments. Simulations of the magnetorefractive effect for the Co/Cu multilayer samples are presented as a function of the wavelength in Figs. 4 and 5.

In setting appropriate parameters for simulating the MRE it is useful to distinguish those that are characteristic of the Co/Cu system in general, i.e., approximately constant for all samples, and parameters such as thickness and m_0 that vary significantly from sample to sample. In this simple two channel model the latter values define the interlayer coupling and mainly control the differences in the GMR of different samples. However, the materials parameters influence both τ_{sal} and β_{sal} which affect both the magnitude and the shape of the MRE. This is illustrated in Fig. 4 where the MRE profile

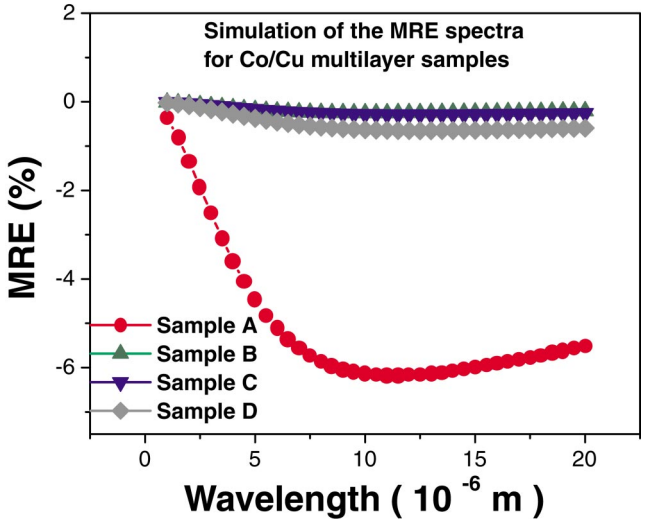

FIG. 5. (Color online) Theoretical simulation of the MRE spectra in a saturating applied field.

is predicted for a range of τ_{sal} and β_{sal} values assuming saturation ($m=1$) with the field on and $m_0=0$ in the absence of a field. Plausible values $\omega_p=1.49\times10^{16}$ s^{-1} and $\varepsilon_{st}=3.5$ are used. The magnitude of the effect increases steadily with increasing β_{sal} as expected [Fig. 4(a)], but both the shape and the magnitude of the profile are strongly influenced by τ_{sal} [Fig. 4(b)]. In the regime $\omega\tau_{sal}\ll1$ the curve tends towards $\Delta R/R\propto\lambda^{-1/2}$ (the Hagen-Rubens regime),[4,6] but for large τ_{sal} this does not set in till large λ. In all cases $\Delta R/R$ tends towards zero as $\lambda\to0$, i.e., when $\omega\tau_{sal}\gg1$. This result can be understood analytically: in the absence of a field, the normal reflectivity R varies as $R=1-2/\omega_p\lambda_{sal}$ so that $\Delta R/R\propto\lambda_{sal}^{-1}$ in the absence of a field (see Ziman[20]). Since λ_{sal}^{-1} is independent of spin, the MRE vanishes in that limit. The shape of the MRE vs λ curve is very strongly dependent on τ_{sal} with a sharp minimum at low τ_{sal} (6×10^{-16} s), a broad minimum with a sharp drop to zero at intermediate τ_{sal} (3×10^{-15} s) and the much reduced scale of the effect at larger τ_{sal} (10^{-14} s).

β_{sal} and τ_{sal} are dependent on a balance of spin-dependent and spin-independent processes. In simulating the experimental results the following parameters were chosen: $\omega_p=1.43\times10^{16}$ s^{-1} corresponding to an average of $n=6.5\times10^{28}$ m^{-3} electronic concentration, $\tau_f=\tau_{Co}=1.2\times10^{-14}$ s, $\tau_n=\tau_{Cu}=2.5\times10^{-14}$ s, and $\tau_i=0.18\times10^{-14}$ s. The spin asymmetry coefficients in the bulk ($\beta=0.6$) and at the interface ($\gamma=0.8$) are consistent with the values reported in literature for Co/Cu multilayers.[18,21] As the dominant spin-dependent scattering is likely to take place at the interface rather than in bulk, this was expressed by taking $\tau_i<\tau_f$. The interface region is assumed to be 5.6 Å (approximately two atomic layers) so that layer thicknesses are small and the importance of interface spin-dependent scattering is reinforced.[22] The above parameters combine with thickness data (Table I) to determine τ_{sal} and β_{sal}. The shape of the MRE curve is very sensitive to the value of τ_i as amplified above. Shorter values produce a pronounced minimum of the MRE at short wavelengths inconsistent with the experimen-

tal data. Increasing the value of τ_i reduces the MRE magnitude to values well below those found experimentally.

The main difference between the samples was the thickness of the Cu interlayers leading to different interlayer exchange coupling related to m_0 as well as different interface volume fractions. A combination of high spin-dependent scattering at the interface ($\gamma \rightarrow 1$) and strong antiferromagnetic coupling ($m_0 \rightarrow 0$) gives the highest GMR and MRE values for sample A, while weak antiferromagnetic coupling ($m_0 \rightarrow 1$) gives a lower GMR/MRE in the sample B and C (see the values m_0 in Table I). Sample D represents an intermediate case. The simulations successfully reproduce the general shape of the wavelength dependence of the MRE for all samples at other than short wavelengths (see Figs. 2 and 5) with a plausible but not necessarily definitive set of parameters. A good quantitative comparison is obtained for the high MRE/GMR sample A in the medium to high wavelength region. At low MRE/GMR the comparison is extremely sensitive to m_0 as m_0 approaches unity. Furthermore at low magnetoresistance other magnetoresistive mechanisms (not accounted for in the GMR model) may be important and so quantitative correlation is less precise.

The effective medium approximation may have its limitations in simulating the magnitude of the effect and the size of the MRE effect is also highly sensitive to geometry at high angles of incidence. In addition, the shape of the spectra at short wavelengths is not well represented by this Drude model and fails to produce the cross-over of the MRE from positive to negative values. The JV model is formulated in terms of Drude-like spin-dependent scattering rates and has to be compared with more sophisticated descriptions of the GMR process, for example, as discussed by Tsymbal and Pettifor.[23] Recently, Baxter *et al.*[13] have adapted a GMR theory involving an orthogonal tight binding (TB) approximation to calculate the MRE of the Co/Cu system investigated here. The tight binding parameters take the form of on site energy levels and hopping integrals of Slater-Koster form. The spin-dependent band structures of the multilayer systems investigated here are calculated using Co and Cu band parameters fitted to *ab initio* band structures of the elemental metals with Co—Cu bond values taken as the geometric mean of those for Co—Co and Cu—Cu. The optical conductivity is then calculated using the Kubo-Greenwood formula. Scattering rates do not appear explicitly within the formalism, but both intraband and interband excitations are included: the parameters used are in no sense fitted to the MRE. These first principle calculations show that interband transitions start to become very important below a wavelength of about 3 μm (Ref. 13) and it is therefore expected that a classical Drude modified model will breakdown as the wavelength is reduced. When the conductivity is decomposed into competing contributions from intraband (Drude-like) and interband effects a change of the sign in the MRE at short wavelengths may occur as in the data presented here (see Fig. 2), emphasizing the need for a full energy band input into model of the MRE.[13] Interband contributions are not as important at long wavelengths where Hagen-Rubens-like behavior is reproduced, but they have the effect of modifying the effective Drude parameters in a JV style model.

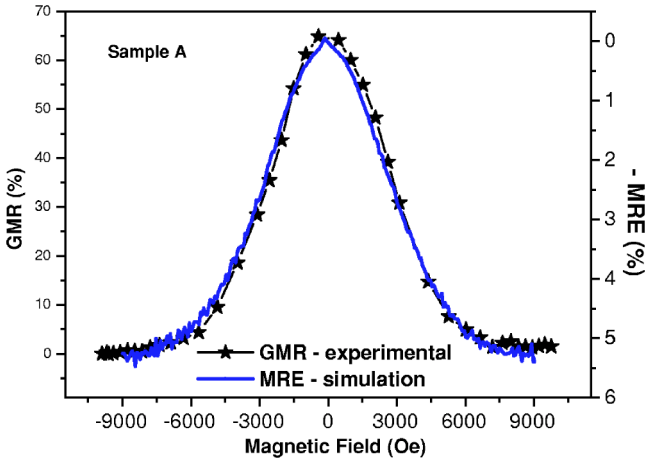

FIG. 6. (Color online) Simulation for sample A (t_{Cu}=7.5 Å) of the MRE at fixed wavelength (20 μm) as a function of the applied field.

Measurement of a full magnetotransport profile, using MRE as a function of the applied magnetic field and wavelength, is time consuming and inconvenient for practical applications. A solution to this problem would be the implementation of a fixed wavelength IR reflection experiment by using, for example, an IR CO_2 laser or other medium to long wavelength source. The experiment could be performed efficiently by directly recording the changes in the reflected IR beam as a function of the applied magnetic field, which is varied between a maximum value and zero. Initial theoretical studies of MRE at fixed wavelength confirm that the MRE follows the same profile as the GMR with respect to the applied field (see Figs. 6 and 7). The simulated MRE profile as a function of the applied field is directly obtained by applying the relation (13) except that in relations (3), (11), and (12) the wavelength is now kept constant and m is varied as a function of the applied magnetic field. The m values were taken directly from the experimental normalized magnetic hysteresis loops. It has previously been shown[6] that the correlation between the GMR and the MRE should be most

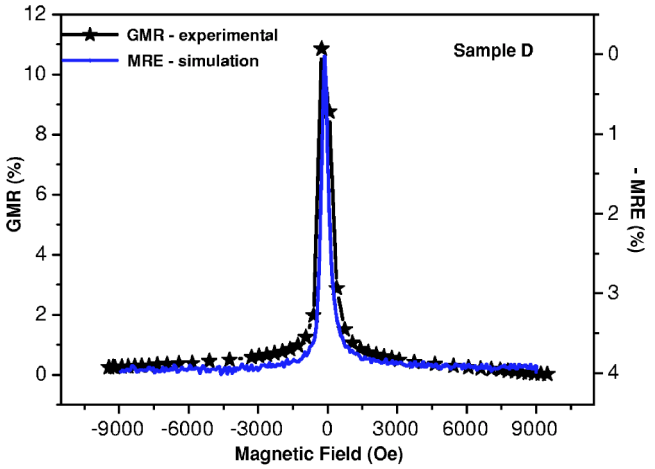

FIG. 7. (Color online) Simulation for sample D (t_{Cu}=16.7 Å) of the MRE at fixed wavelength (20 μm) as a function of the applied field.

direct at long wavelengths, i.e., in the Hagen-Rubens limit when $\omega\tau_{sal} \ll 1$. Consequently the Drude model should be capable of reproducing the maximum values of the MRE measured at long wavelengths and predicting the variation of the MRE as a function of the applied field. We have simulated the MRE profile as a function of the applied magnetic field at a constant wavelength of $\lambda = 20$ μm using the same simulation parameters as those given earlier in this section. The simulated MRE as a function of the applied magnetic field was then directly compared with the experimental GMR data, showing an excellent correlation for the full range of the applied magnetic field (Figs. 6 and 7).

Note that the correlation between GMR and MRE is insensitive to the precise choice of wavelength except for the value of the constant of proportionality. This makes the MRE a robust technique for the measurement of GMR profiles. These graphs together with Fig. 3 clearly show the possibility of performing noncontact magnetotransport measurements on magnetoresistive samples by measuring the variation of their infrared reflected intensity at fixed λ when a magnetic field is applied.

VI. CONCLUSIONS

The magnetotransport properties of giant magnetoresistive Co/Cu multilayers have been studied using the magnetorefractive effect. A direct correlation between the experimental MRE in the mid to far infrared regime and the electrically measured GMR was observed. The shape and magnitude of the experimental MRE curves were modeled using the complex dielectric function as derived by Jacquet and Valet.[1] This classical model was successful in simulating the long wavelength behavior and the variation of the MRE as a function of the applied field with plausible materials parameters. The shape of the MRE curves was found to be very sensitive to the value of τ_i, the interface scattering lifetime. However the model is not able to fully reproduce the shape of the spectra at short wavelengths demonstrating the need for a theoretical approach capable of incorporating the band structure of the multilayers. The excellent empirical correlation between the simulated MRE at 20 μm and the electrical GMR as a function of magnetic field (Figs. 6 and 7), coupled with the correlation between the maximum MRE and GMR values (Fig. 3), demonstrate the potential of using the MRE to perform fast *in situ* noncontact magnetotransport measurements, especially at fixed infrared wavelength.

ACKNOWLEDGMENTS

The financial support of the Engineering and Physical Sciences Research Council and Seagate Technology—Northern Ireland is gratefully acknowledged.

*Present Address: York EMC Services Ltd, University of York, Heslington YO10 5DD, UK.

†Present Address: Oxford Applied Research, Crawley Mill, Witney, Oxon. OX299SP, UK.

[1] J.C. Jacquet and T. Valet, *Magnetic Ultrathin Films, Multilayer and Surfaces*, edited by E. Marinero (Materials Research Society, Pittsburgh, 1995).

[2] S.D. Bader and J.L. Erskine, *Ultrathin Magnetic Structures*, edited by B. Heinrich and J.A.C. Bland (Springer-Verlag, Berlin, 1994), Chap. 4.

[3] R.M. Osgood III, S.D. Bader, B.M. Clemens, R.L. White, and H. Matsuyama, J. Magn. Magn. Mater. **182**, 297 (1998).

[4] S. Uran, M. Grimsditch, E. Ł. Fullerton, and S.D. Bader, Phys. Rev. B **57**, 2705 (1998).

[5] M. Gester, A. Schlapka, R.A. Pickford, S.M. Thompson, J.P. Camplin, J.K. Eve, and E.M. McCash, J. Appl. Phys. **85**, 8 (1999).

[6] V.G. Kravets, D. Bozec, J.A.D. Matthew, S.M. Thompson, H. Menard, A.B. Horn, and A.F. Kravets, Phys. Rev. B **65**, 054415 (2002).

[7] A.B. Granovskii, M.V. Kuzmichev, and J.P. Clerc, J. Exp. Theor. Phys. **98**, 5 (1999).

[8] D. Bozec, V.G. Kravets, J.A.D. Matthew, S.M. Thompson, and A.F. Kravets, J. Appl. Phys. **91**, 8795 (2002).

[9] A.B. Granovsky, I.V. Bykov, E.A. Ganshina, V.S. Gushchin, M. Inue, Yu. E. Kalinin, A.A. Kozlov, and A.N. Yurasov, J. Exp. Theor. Phys. **96**, 1104 (2003).

[10] J. van Driel, F.R. de Boer, R. Coehoorn, G.H. Rietjens, and E.S.J. Heuvelmans-Wijdenes, Phys. Rev. B **61**,15321 (2000).

[11] M. Vopsaroiu, J.A.D. Matthew, K.A. McNeill, and S.M. Thompson, IEEE Trans. Magn. **39**, 2830 (2003).

[12] R.F.C Marques, P.R. Abernethy, J.A.D. Matthew, and S.M. Thompson, J. Magn. Magn. Mater. **272–276**, 1740 (2004).

[13] R.J. Baxter, D.G. Pettifor, E.Y. Tsymbal, D. Bozec, J.A.D. Matthew, and S.M. Thompson, J. Phys.: Condens. Matter **15**, L695 (2003).

[14] A.M. Fox, *Optical Properties of Solids* (Oxford University Press, Oxford, 2001).

[15] H.P. Myers, *Introductory Solid State Physics* (Taylor and Francis, New York, 1997).

[16] S. Zhang and P.M. Levy, J. Appl. Phys. **69**, 8 (1991).

[17] S. Zhang, Appl. Phys. Lett. **61**, 1855 (1992).

[18] T. Valet and A. Fert, Phys. Rev. B **48**, 7099 (1993).

[19] E. Hecht, *Optics*, 3rd ed. (Addison Wesley, New York, 1998).

[20] J.M. Ziman, *Principles of the Theory of Solids* (Cambridge University Press, Cambridge, 1964).

[21] P. Holody, W.C. Chiang, R. Loloee, J. Bass, W.P. Pratt, and P.A. Schroeder, Phys. Rev. B **58**, 12 230 (1998).

[22] A. Barthelemy, A. Fert, J-P. Contour, M. Bowen, V. Cros, J.M. De Teresa, A. Hamzic, J.C. Faini, J.M. George, J. Grollier, F. Montaigne, F. Pailloux, F. Petroff, and C. Vouille, J. Magn. Magn. Mater. **68**, 242 (2002).

[23] E.Y. Tsymbal and D.J. Pettifor, Solid State Phys. **56**, 113 (2001).